Kaufmann, G., Wu, P., Wolf, D. (1997): Some effects of lateral heterogeneities in the upper mantle on postglacial land uplift close to continental margins. - Geophysical Journal International, 128, 1, pp. 175—187.

DOI: https://doi.org/10.1111/j.1365-246X.1997.tb04078.x

Geophys. J. Int. (1997) **128,** 175–187

Some effects of lateral heterogeneities in the upper mantle on postglacial land uplift close to continental margins

G. Kaufmann,[1,*] P. Wu[2] and D. Wolf[3]
[1]*Research School of Earth Sciences, Australian National University, Canberra, Australia*
[2]*Department of Geology and Geophysics, University of Calgary, Calgary, Alberta, Canada*
[3]*GeoForschungsZentrum Potsdam, Division 1: Kinematics and Dynamics of the Earth, Potsdam, Germany*

Accepted 1996 August 30. Received 1996 August 28; in original form 1995 October 31

SUMMARY

We investigate the effects of lateral heterogeneities in the upper mantle on the calculation of postglacial land uplift. For the model calculations we use a commercial finite-element code, which enables us to solve the equations governing a layered, isotropic, incompressible, Maxwell-viscoelastic half-space with laterally varying layer thicknesses and physical properties. Following previous investigations performed by Sabadini, Yuen & Portney (1986) and Gasperini & Sabadini (1989), we extend their results using a more realistic loading history and different earth models. We then focus our attention on the question whether lateral heterogeneities in the upper mantle can be modelled correctly using a set of homogeneous earth models. To this end, a comparison of model calculations using both laterally homogeneous and heterogeneous earth models is performed.

We find that lateral heterogeneities in the upper mantle significantly influence the calculated postglacial land uplift. The resolving power of relative sea-level observations for the prescribed lateral heterogeneities used in this study is mainly focused on observations around the load margin and outside the glaciated areas, where differences in predicted land uplift between individual models are large enough to be resolved by observations.

We can qualitatively determine lateral heterogeneities in the upper mantle using a set of laterally homogeneous earth models, if the geological structure, for example a continental margin, is known. However, in order to infer the correct values of lithospheric thickness and asthenospheric viscosity, we need to use laterally heterogeneous models.

Key words: asthenosphere, continental margins, glacial rebound, lateral heterogeneity, lithosphere.

1 INTRODUCTION

The Earth as a dynamical body undergoes changes caused by a variety of forces, for example the gravitational attraction by planetary bodies, the driving forces related to mantle convection, and the loading forces by volcanoes and ice sheets. As a result of these forces, the Earth changes its shape (mountain building, postglacial rebound), its gravitational potential (sea-level change), its stress field (tectonics), and its rotation (polar wander, changes of length of day).

The response of the Earth to these forces can be studied by a variety of geophysical observations. One important phenomenon is *postglacial land emergence*. This is caused by the global redistribution of ice and water related to the last glaciation cycle of the Pleistocene ice age and the mass redistribution in the Earth's mantle.

The concentration of ice in regions close to the poles and the redistribution of ocean water to continental ice sheets resulted in significant changes in the Earth's shape and gravitational potential. In the formerly glaciated areas the ice sheets caused significant deformation of the Earth's surface. Near the centres of the Canadian (Hudson Bay) and Fennoscandian ice sheets (Ångermanland), this led to several hundreds of metres of land submergence. Due to mass conservation the growth of the ice sheets resulted in a global fall of sea level by about 130 m, the missing water forcing the bottom of the oceans to rise slightly.

The melting of the Pleistocene ice sheets reversed the effects

* Corresponding author.

mentioned above. The sea reached its original level by about 6 ka BP, when most of the Pleistocene ice sheets had melted. However, the movement of the Earth's surface continues due to the delayed viscous relaxation of the Earth's mantle.

The first correct interpretation of postglacial land emergence in formerly glaciated areas was given by Jamieson (1865), who described it as a rebound of the land following the melting of the ice sheets. Daly (1934) emphasized that the delayed relaxation of the Earth's surface is strongly controlled by the rheology of the Earth's mantle, which behaves like a viscous fluid on timescales typical of glaciations. Based on these ideas, Haskell (1935) and van Bemmelen & Berlage (1935) presented model calculations for a Newtonian viscous fluid to explain the structure and viscosity of the Earth's mantle. McConnell (1968) introduced an elastic layer to mimic the influence of the Earth's lithosphere on postglacial land emergence.

In more recent interpretations of postglacial land emergence, the thickness of the elastic lithosphere, as well as the viscosity of the Earth' mantle, has received particular attention (Wolf 1993). The earth models used were usually layered, *viscoelastic* half-spaces or spheres, which can explain both the instantaneous (elastic) deformation and the delayed (viscous) relaxation of the Earth in response to applied surface loads (e.g. Peltier 1974; Cathles 1975; Wolf 1987; Nakada & Lambeck 1989; Lambeck, Johnston & Nakada 1990; Tushingham & Peltier 1991, Mitrovica & Peltier 1992; Fjeldskaar 1994). A common feature of these earth models is that the material properties (density, shear modulus, viscosity, layer thickness) do not vary laterally. However, it is not clear *a priori* whether the interpretation of postglacial land emergence can be based on laterally homogeneous earth models. This is because other geophysical observations require lateral variations of the material properties. In particular, the inversion of seismic *S*-wave velocities (Woodhouse & Dziewonski 1984; Tanimoto 1990; Nataf & Ricard 1996) has resolved lateral variations in the upper mantle down to a size of 2000 km. The results show that there are regions in the upper mantle with reduced (central and southwestern Pacific, Tasman Sea) and increased (North America, parts of northern Europe) *S*-wave velocities. The variations have been related to hotter regions under mid-ocean rift zones and colder regions under tectonically stable cratons. In view of the exponential dependence of viscosity on temperature, this is expected to lead to pronounced lateral variations of viscosity, if the seismic velocities arise from thermal anomalies alone. Strong lateral variations of the viscosity of the mantle also result from numerical simulations of mantle convection with temperature-dependent viscosity (Nataf & Richter 1982).

The influence of lateral heterogeneity on postglacial land emergence was studied by Sabadini *et al.*(1986), Sabadini & Gasperini (1989), and Gasperini, Sabadini & Yuen (1991). The authors concluded that a variation of lithospheric thickness mainly influences the land emergence near the margins of former ice sheets, whereas the land emergence near their centres is relatively insensitive to such variations. Gasperini & Sabadini (1989) studied in particular the influence of lateral viscosity variations on postglacial land emergence. For an ice load comparable in size with the former Fennoscandian ice sheet they considered an earth model with a harmonic variation of viscosity. The wavelength of the variation was similar to the size of a convection cell, and the double amplitude was up to two decades. The results of their calculations showed that this earth model can explain the postglacial land emergence in Fennoscandia equally as well as an earth model with laterally homogeneous model parameters.

Lateral variations of mantle viscosity on a global scale were inferred by Nakada & Lambeck (1991), who modelled worldwide sea-level changes caused by the melting of the Pleistocene ice sheets. They suggested that the viscosity is lower below the southwestern Pacific, Tasmania, and eastern Australia than under North America and Europe.

Breuer & Wolf (1995) interpreted the land emergence in the Svalbard Archipelago, a group of islands in the European Arctic close to the continental margin. They concluded that the observed land emergence suggests increasing lithospheric thickness and asthenospheric viscosity towards the Eurasian continent.

Kaufmann & Wolf (1996) have proposed an extended interpretation of the land emergence in the northern Barents Sea using the high-resolution ice model BARENTS-2 and observations from 25 locations. Whereas the results essentially confirm those due to Breuer & Wolf (1995), they show more clearly that the interpretation of the postglacial land emergence only indicates lateral variations in the asthenospheric viscosity.

It is important to note that in the investigations of Nakada & Lambeck (1991), Breuer & Wolf (1995), and Kaufmann & Wolf (1996) the inference of lateral heterogeneities was based on the interpretation of postglacial land emergence with a set of laterally homogeneous earth models. However, it has not yet been demonstrated that laterally homogeneous earth models can in fact be used to investigate lateral heterogeneities in the Earth's mantle. Thus, one of the purposes of this paper is to investigate whether the inferred lateral variations in lithospheric thickness and asthenospheric viscosity (from laterally homogeneous models) truly reflect the prescribed variations for a load whose dimensions are comparable to the Fennoscandian ice sheet. This is an important question, because the validity of such a method could potentially reduce the need for modelling postglacial land emergence with laterally heterogeneous earth models.

With the above purpose in mind, the plan of this paper is as follows. In Section 2 we introduce the model we have used to calculate vertical displacements. In Section 3 we present the results of our model calculations. In Sections 3.1 and 3.2 we investigate the response of earth models with lateral heterogeneities in the lithosphere and asthenosphere to surface loading for two simple loading histories. A jump in lithospheric thickness in Section 3.1, as a simple approximation of a continental margin, is a first step towards the physical understanding of discontinuities in earth models. The results of Section 3.1 can also be used to calibrate our model and to compare our calculations with those by Sabadini *et al.* (1986). In Section 3.2, more realistic earth models with smoother lateral variations of lithospheric thickness and asthenospheric viscosity are used. These models provide improved insight into the possibility of resolving lateral heterogeneities in the upper mantle using observations of postglacial land uplift. Based on these models, we investigate in Section 3.3 the validity of using sets of laterally homogeneous earth models to resolve lateral variations, as done in Breuer & Wolf (1995) and Kaufmann & Wolf (1996). We conclude this paper by summarizing our results in Section 4.

2 THEORETICAL MODEL

We are interested in the inference of lateral heterogeneities from postglacial rebound in regions close to a continental margin like Scandinavia and the Barents Sea, and thus the earth model considered is a layered, isotropic, incompressible, Maxwell-viscoelastic half-space. The gravitational acceleration g and the density ρ of the half-space are kept fixed. The flat-earth approximation has been demonstrated to be adequate for describing the rebound process for loads with size smaller than or comparable to the Fennoscandian ice sheet (Wolf 1984; Amelung & Wolf 1994) and is therefore adopted. Since our focus is on the effect of lateral heterogeneities on land emergence in Scandinavia, the earth model is kept as simple as possible and features an incompressible material and no rheological stratification below the upper mantle. The latter is justified by the poor resolving power of observational data in the lowermost mantle (Mitrovica & Peltier 1993). The validity of using incompressible earth models for interpretating postglacial rebound observations has been shown by Wolf (1985a). The assumption of uniform viscosity in the upper and lower mantle for modelling postglacial land emergence in Scandinavia and the Barents Sea has also been demonstrated to be valid by (Wolf 1987), Fjeldskaar (1994), and Kaufmann & Wolf (1996).

In this study, the engineering-oriented commercial finite-element package ABAQUS has been used to calculate the deformations. The problem to be solved by the finite-element (FE) method is similar to the Boussinesq problem for a layered, viscoelastic half-space (Peltier 1974), except that buoyancy forces are included so that the deformed free surface of the Earth is allowed to return to its initial state via viscous flow. Thus, the equation that describes the conservation of momentum is given by (e.g. Cathles 1975, eq. III-3):

$$\nabla\cdot\boldsymbol{\sigma} - \rho g \nabla w = 0, \qquad (1)$$

where $\boldsymbol{\sigma}$ is the incremental stress tensor and w is the vertical displacement. The first term in eq. (1), the divergence of stress, describes the surface force deforming the Earth. The second term arises because the undisturbed Earth is assumed to be in hydrostatic equilibrium, with the forces of self-gravitation balanced by the hydrostatic pre-stress. As discussed in Love (1911), Cathles (1975) and Wolf (1991), this pre-stress is being advected along with the material when the body deforms either elastically or viscoelastically. Thus, the second term in eq. (1) represents the gradient of the advected pre-stress, $\rho g w$. The presence of this term is required in order to provide the buoyancy force that is needed to satisfy the boundary conditions in the fluid limit (Wu & Peltier 1982), and without this term there would be no viscous gravitational relaxation (Wu 1992a,b). The incorporation of pre-stress advection into finite-element codes has been discussed by Gasperini & Sabadini (1989). Details about the adaptation of ABAQUS to Earth deformation calculations can be found in Spiteri (1991).

After an extensive study of the optimal element size, aspect ratio and boundary effects, the following finite-element scheme has been adopted. The earth model is represented by 15 layers, each of which has 40 axi-symmetric 4-node bilinear solid elements and one boundary element that extends to infinity. The disc load covers 10 elements at the surface. The last solid element on each layer, which attaches to the boundary element, is located at a distance 20 times larger than the radius of the load.

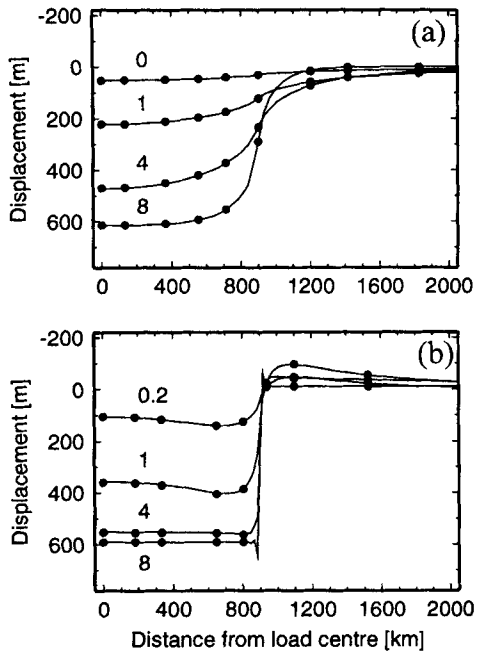

Figure 1. Vertical displacement as a function of distance from the load centre for a Heaviside response and the finite-element method (lines) and the Hankel transform method (filled circles). The earth models used are a viscoelastic half-space (a) and a 420 km thick viscoelastic channel (b). The numbers by the curves are times after the Heaviside loading in ka.

The grid is not evenly spaced, being densest near the edge of the load.

The validity of the FE method is shown in Fig. 1, where the Heaviside step response of Maxwell-viscoelastic earth models calculated with the FE method is compared with that calculated with the conventional Hankel transform method (see Wu 1993). In Fig. 1(a) the earth model used is a viscoelastic half-space. Here the results of the FE method (lines) and the conventional method (filled circles) are in excellent agreement. The differences are within 0.6 per cent underneath the load. In Fig. 1(b) a viscoelastic channel is used. Here the results are also usually in excellent agreement for the two methods. However, the FE method breaks down near the edge of the load for $t > 4$ ka, because the stress gradient is too steep at the load margin. Fortunately, this problem does not arise in a real Earth, because an elastic lithosphere always exists at the surface and this smoothes the stress gradient and ensures an acceptable FE solution near the edge.

3 RESULTS FOR SIMPLE EARTH MODELS

In this section we present some results of our model calculations. We have investigated the response of a laterally heterogeneous, viscoelastic, layered half-space for two different loading histories. The applied surface load for all calculations is a parabolic disc with a radius of 800 km, a density of 1000 kg m^{-3}, and a maximum height of 2500 m at the centre. Like Gasperini & Sabadini (1989), we regard these dimensions as comparable with the Fennoscandian ice sheet. The loading histories used in the following sections model a Heaviside unloading event and a linear loading cycle (Fig. 2).

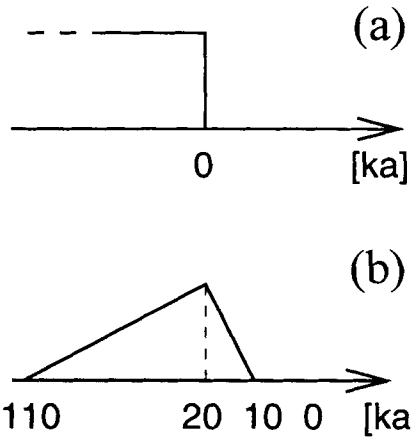

Figure 2. Sketches of loading histories used in this study. The Heaviside unloading event (a) describes an instantaneous unloading at time $t = 0$. The linear loading cycle (b) represents a smooth growing of the ice load over 90 ka, followed by a rapid deglaciation over 10 ka, which ended at 10 ka BP.

3.1 Heaviside unloading

The results in this section all apply for a surface load, which has deformed the viscoelastic half-space for an infinite time and which is then instantaneously removed at time $t = 0$. For this *Heaviside unloading event*, the deformation has reached isostatic equilibrium before the removal of the load.

We have used two *laterally homogeneous* reference models consisting of a 150 km (H01) and a 50 km (H02) thick elastic lithosphere overlying a viscoelastic mantle. These models, which are shown in Fig. 3, can be regarded as simple approximations for earth models with a thick *continental* (H01) and a thin *oceanic* (H02) lithosphere. To investigate the effect of lateral variations in lithospheric thickness on the calculated land emergence, we have used several *laterally heterogeneous* two-layer models consisting of an elastic lithosphere overlying a viscoelastic mantle. The thickness of the lithosphere h_1 is given through a step function, with a 150 km thick lithosphere under the load and a 50 km thin lithosphere further out. The distance at which the lithospheric thickness changes abruptly is called the *step distance* l. We have chosen steps at 400 km (HV1), 800 km (HV2), and 1200 km (HV3). We also consider a linear decrease in lithospheric thickness from 150 km at the load centre to 50 km at a distance of 1200 km (HV4). The models are shown in Fig. 3, and their physical properties are given in Table 1.

In Figs 4 and 5 we show the effect of a lateral variation in the lithospheric thickness. In Fig. 4 the *vertical displacements* for the models H01 (dotted line) and H02 (dashed line) are compared with the displacements for the laterally heterogeneous models HV1–HV4. Fig. 4 demonstrates well the effect of a thicker lithosphere, which spreads the deformation farther away from the load and decreases its amplitude both underneath the load and in the forebulge. A closer inspection of Figs 4(a)–(c) shows that three areas can be distinguished. Close to the load centre, all laterally heterogeneous models can be replaced by the continental reference model H01. Far away from the load centre, the oceanic reference model H02 is a better approximation of the laterally heterogeneous models. The third area, which is called the *transitional range*, is the area close to the step distance. Here the lateral heterogeneity

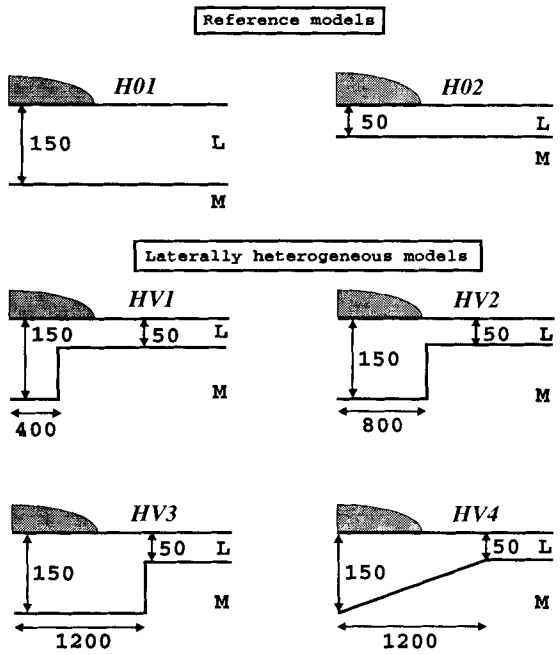

Figure 3. Sketches of earth models used for the Heaviside unloading event. The symbols L and M denote lithosphere and mantle. The numbers are lengths in km.

clearly influences the relaxation process. In Fig. 4(a) the step distance is $l = 400$ km; as a consequence, the relaxation changes from 'continental' to 'oceanic' behaviour 200–500 km from the load centre. For model HV2 with a step distance directly at the load margin ($l = 800$ km), the transitional range is located at 700–1000 km. A step distance at 1200 km (model HV3) shifts the transitional range to 1100–1400 km. For all three models the influence of the lateral variation in lithospheric thickness is relatively sharp and focused on the range ± 150 km around the step distance. In contrast to this, the relaxation of model HV4, with its linear decrease in lithospheric thickness, shows a transition zone extending over the entire area where the lithospheric thickness varies.

In Fig. 5 we have modelled the *land uplift* history for several models. As a reference point, we have chosen the present time to be 13 ka after the load removal; by this time all models have reached at least 90 per cent of their new hydrostatic equilibrium. The results are shown for the load centre ($r = 0$ km) and for distances $r = 600$, 800 and 1000 km.

At the load centre (Fig. 5a), the land uplift for models HV1–HV4 is similar to the land uplift for the continental reference model H01. Here the influence of the thick continental root dominates the uplift. At $r = 600$ km (Fig. 5b), the percentage differences between the land uplift of the two reference models are small. This shows that the lithospheric thickness cannot be clearly resolved by the laterally heterogeneous models at this particular location. At the load margin for $r = 800$ km (Fig. 5c), the percentage differences between the land uplift for the laterally heterogeneous and homogeneous models are larger. The land uplift above the thinner part of the lithosphere of model HV1 can be calculated using the oceanic reference model H02. On the other hand the land uplift for the continental reference model H01 is a good approximation of the land uplift for model HV3, because here the observation site is

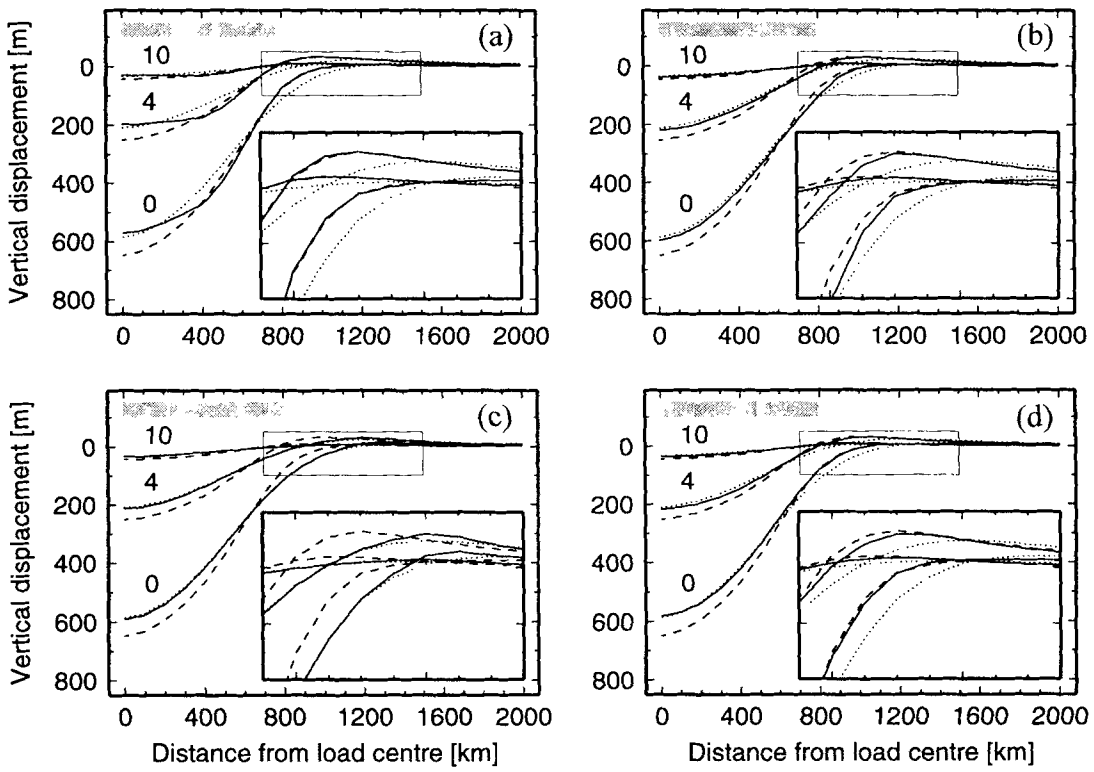

Figure 4. Vertical displacement as a function of distance from the load centre for the reference models H01 (dotted) and H02 (dashed) and the laterally heterogeneous models HV1 (a), HV2 (b), HV3 (c), and HV4 (d) (solid). The numbers by the curves are times after load removal in ka. The shaded bars indicate the radial extension of the load; the areas enclosed by the rectangle are shown as enlargements.

located above the thicker part of the lithosphere. The thinner lithosphere, which begins 400 km farther out, has an insignificant influence on the relaxation process. For model HV2, the observation site at $r = 800$ km is located directly above the step distance; the land uplift is therefore between the uplifts for the reference models. A similar behaviour can be observed for model HV4. Here the observation site is located above part of the lithosphere that is 83 km thick; the land uplift for this model consequently lies between those for the two reference models. In fact, for most sites within and outside the ice margin, these two models give similar results. Thus, a sharp change in lithospheric thickness can be used to approximate a linear change in lithospheric thickness. However, the disadvantage is that sharp changes and gradual changes cannot be distinguished clearly.

At $r = 1000$ km (Fig. 5d), the land uplift for models HV1, HV2, and HV4 can be approximated by the land uplift of the oceanic reference model H02. Here the observation sites are located above the thinner parts of the lithosphere. The thicker continental root under the load has an insignificant influence on the calculated land uplift. For model HV3, the observation site is located above the thicker part of the lithosphere; therefore, the land uplift is approximately the same as for the continental reference model H01.

We can directly compare some of our results with calculations by Sabadini *et al.* (1986), where the authors investigated the effect of a 150 km thick continental lithospheric root underlying a glacial load on postglacial land uplift. The lithosphere outside the formerly glaciated area was kept fixed at 50 km. Sabadini *et al.* (1986) used a parabolic disc load with a radius of 1668 km, a maximum load height of 3 km, and a Heaviside unloading event. The dimension of their load is comparable with the Laurentide ice sheet over Canada.

Sabadini *et al.* (1986) concluded that the land uplift of their model at the load centre is similar to the uplift resulting from a model with a uniformly thick lithosphere of 150 km. Our results shown in Fig. 5(a) and discussed above confirm their conclusion for a smaller load. Sabadini *et al.* (1986) have found significant differences in land uplift in the peripheral bulge and in the far-field, when comparing the model with a thick continental root to a reference model with a uniformly thin lithosphere of 50 km. They report a decrease of the peripheral bulge of about 50 per cent relative to the reference model. We obtain a similar reduction of the peripheral bulge when comparing our models HV3 and H02 in Fig. 5(d). Here the maximum uplift for model HV3 has decreased by about 60 per cent relative to model H02. The close agreement in the relative reduction, despite the difference in the size of the load, provides further confidence in our results. We therefore regard this comparison as a further check of our approach.

Summarizing the results for the Heaviside unloading event, we find that a step in lithospheric thickness results in a transition zone close to the step distance. At the load margin and just outside the load, the differences in the calculated land uplift for different earth models are large enough to be resolved by observations of postglacial land emergence. In the next section we examine the influence of lateral heterogeneities for the more realistic linear loading cycle.

Table 1. Parameters of the earth models.

Layer	Density ρ [kg m^{-3}]	Shear modulus μ [Pa]	Viscosity η [Pa s]	Thickness h [km]
Lithosphere	3380	0.67×10^{11}	∞	h_1
Asthenosphere*	3380	1.45×10^{11}	η_2	h_2
Mantle	3380	1.45×10^{11}	10^{21}	∞

* only for models L01–18, L01–19, LV1–LV4

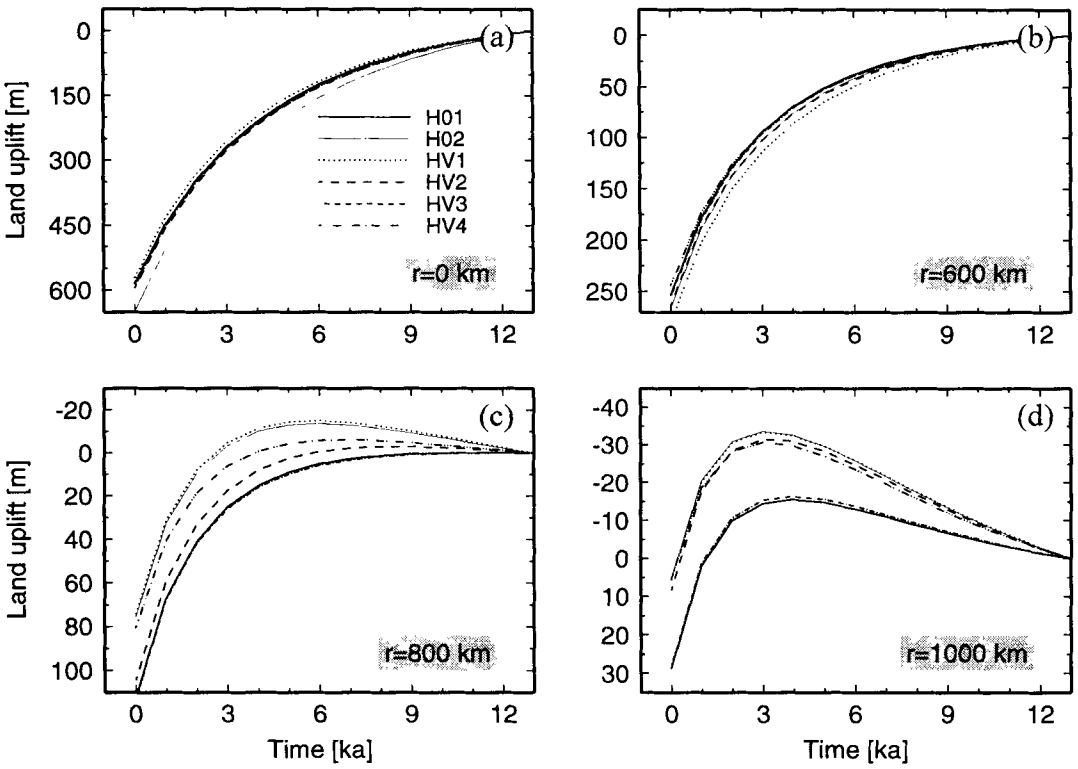

Figure 5. Land uplift as a function of time for models H01, H02, and HV1–HV4 at the observation points $r = 0$ km (a), 600 km (b), 800 km (c), and 1000 km (d). The line styles for the various models are given in (a).

3.2 Linear loading cycle

In this section we present results of model calculations based on smoother lateral variations in the lithosphere and asthenosphere and a linear loading cycle. The loading history is a simple approximation of the Pleistocene glaciation phase, modelling an ice sheet which grows over a period of 90 ka followed by a rapid deglaciation over 10 ka. The parabolic disc load has vanished completely at 10 ka BP. We have used two modified *laterally homogeneous* reference models, one with a 110 km thick continental (L01) lithosphere, and one with a 55 km thick oceanic (L02) lithosphere, both with an underlying viscoelastic mantle. The *laterally heterogeneous* models are as follows. Model LV1 is a two-layer model with an elastic lithosphere and a viscoelastic mantle. The lithospheric thickness is 110 km from the load centre to a distance of 400 km, it decreases linearly to 55 km over a distance of 800 km, and finally remains fixed at 55 km from 1200 km to infinity. Model LV2 is a three-layer model with a 110 km thick elastic lithosphere, a 200 km thick viscoelastic asthenosphere, and a viscoelastic mantle. The viscosity in the asthenosphere decreases stepwise from 10^{21} Pa s under the load to 10^{18} Pa s outside the load every 400 km. Model LV3 combines LV1 and LV2; here both the lithospheric thickness and the asthenospheric viscosity vary laterally. With model LV4 we investigate the effect of a lateral variation in asthenospheric thickness h_2: under a 110 km elastic lithosphere the asthenospheric thickness increases from 60 km at the load centre to 200 km at 1200 km, from there it remains fixed. The asthenospheric viscosity is constant and has a value of 10^{19} Pa s. All models are shown in Fig. 6, and the physical properties are listed in Table 1.

In Fig. 8 the calculated *land uplift* as a function of time BP is shown for the two reference models and the laterally heterogeneous models for four distances. In addition, we have included selected relative sea-level observations and their uncertainties from Scandinavia, corrected for the eustatic

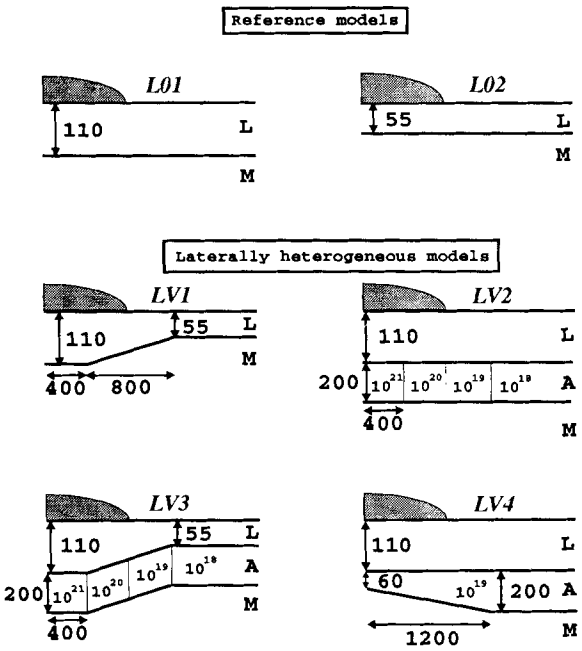

Figure 6. Sketches of earth models used for the linear loading cycle. The symbols **L**, **A**, and **M** denote lithosphere, asthenosphere and mantle. The numbers are lengths in km or asthenospheric viscosities in Pa s.

sea-level change (see Kaufmann & Wolf 1996 for details concerning correction). The geographical location of the observation sites with respect to the parabolic ice load used in the calculations are shown in Fig. 7. The sole purpose of displaying sea-level data is to gain some insight into the question whether the data can be used for discriminating between different earth models. At this stage we are not interested in actually fitting the data with our models.

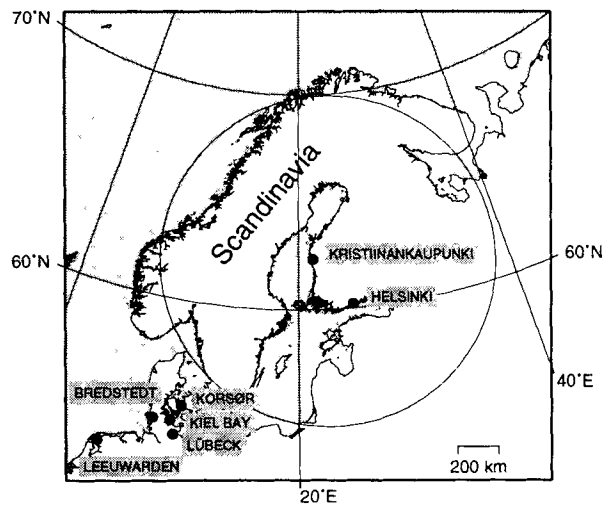

Figure 7. Location map of Scandinavia, showing relative sea-level observation sites used in this study. The circle indicates the approximate location of the disc load.

In Fig. 8(a) the land uplift at the load centre ($r = 0$ km) is shown for all models. We find that the percentage differences

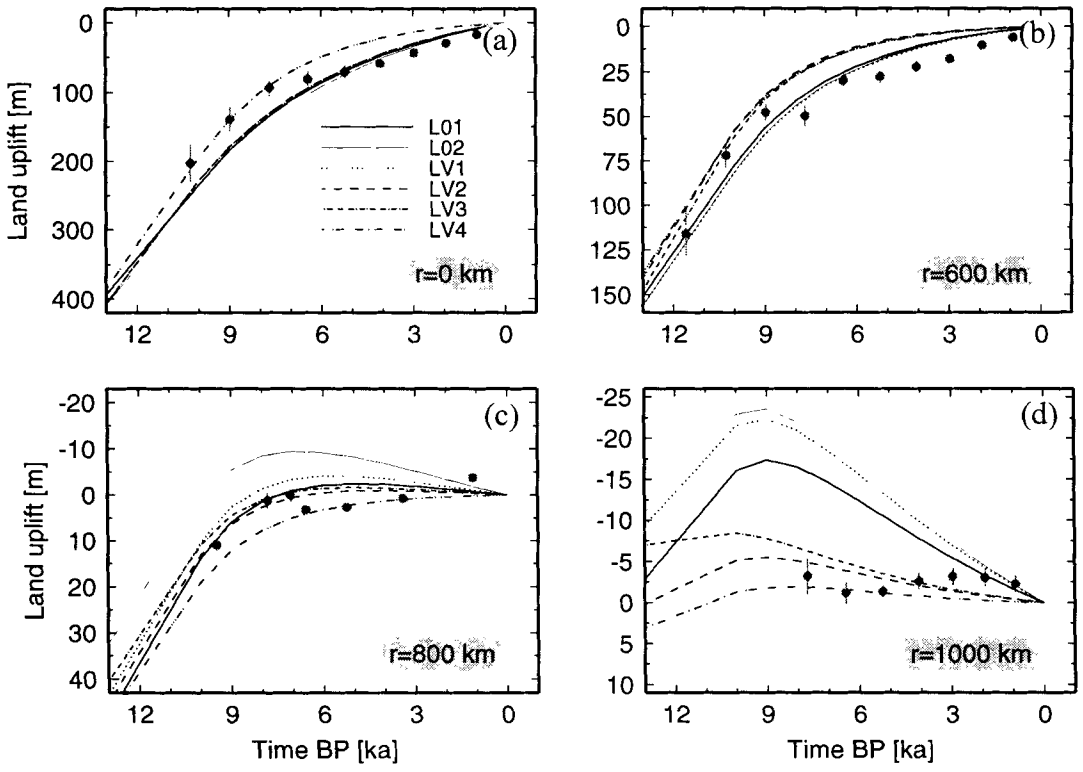

Figure 8. Land uplift as a function of time BP for models L01, L02, and LV1–LV4 at the observation points $r = 0$ km (a), 600 km (b), 800 km (c), and 1000 km (d). The line styles for the models are given in (a). Dots and bars represent observations and related uncertainties for Kristiinankaupunki (a), Helsinki (b), Bredstedt (c), and Lübeck (d).

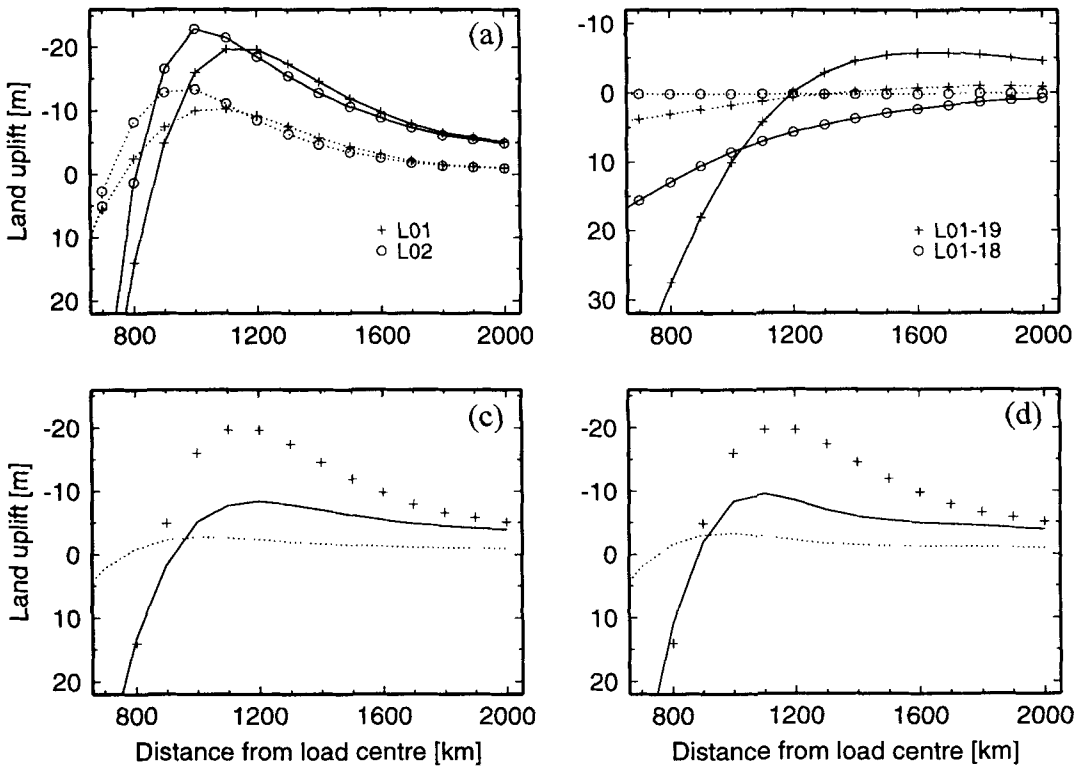

Figure 9. Land uplift in the forebulge area as a function of distance from the load centre at 10 ka BP (solid lines) and 5 ka BP (dotted lines). In (a) and (b) the effects of lithospheric thickness and asthenospheric viscosity on the forebulge development are shown for sets of laterally homogeneous models. Effects arising from lateral heterogeneities in the Earth's mantle are shown for models LV2 (c) and LV3 (d), and compared with model L01 at 10 ka BP (crosses).

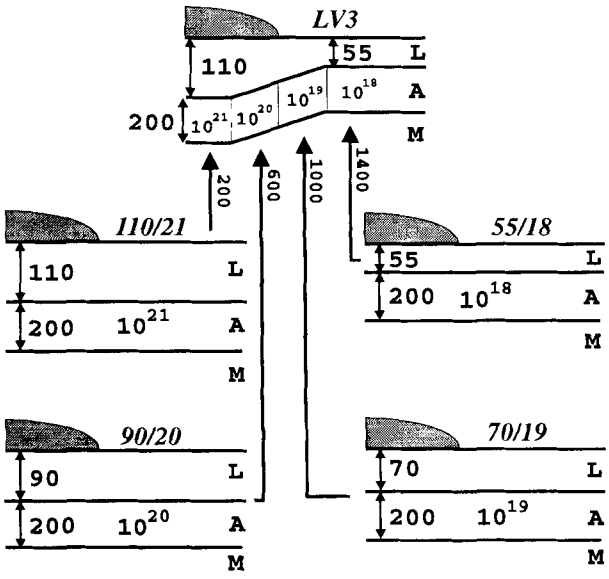

Figure 10. Sketches of earth models used for the comparison. The symbols L, A and M denote lithosphere, asthenosphere and mantle. The numbers are lengths in km or asthenospheric viscosities in Pa s.

for all earth models are very small and thus unresolvable except for model LV4. Here the thin low-viscosity asthenosphere under the load results in significantly shorter relaxation times and therefore a reduced land uplift, an effect which exceeds the observational uncertainties. At $r = 600$ km (Fig. 8b) we can distinguish between two classes of land uplift: models without asthenosphere (L01, L02, LV1) that show larger land uplift and models including an asthenosphere (LV2, LV3, LV4) below the observation point. The type of lateral heterogeneity of the asthenosphere cannot be resolved at this location, indicating that we cannot distinguish between viscosity and thickness variations, despite the poor resolving power for lithospheric thickness at this location. Moving farther out to the load margin at $r = 800$ km (Fig. 8c), the percentage differences in land uplift become more pronounced. In agreement with the intermediate lithospheric thickness of model LV1 at the load margin, the land uplift for this model is between those for the two reference models L01 and L02 (see Section 3.1). A lateral variation in asthenospheric viscosity in model LV2 results in an uplift curve similar to the one of model L01, while an additional lateral variation in lithospheric thickness in model LV3 shifts the land uplift towards that for model L02 for times before 6 ka BP. A significant increase in land uplift relative to that for the continental reference model L01 can be observed for model LV4. In view of the smallness of the observational uncertainties, we can distinguish different rheological models. Outside the load, at $r = 1000$ km (Fig. 8d), the percentage differences in land uplift are even more pronounced. Now the differences in the predictions between deep-flow models resulting in a large forebulge (L01, L02, LV1), pure channel-flow models (LV4), and mixed-flow models (LV2, LV3) clearly exceed the observational uncertainties. Models LV2 and LV3 are considered to be

mixed-flow models, because the asthenospheric viscosity up to a distance of 400 km is equal to the mantle viscosity and thus allows deep flow. At this location the predictions for all models change from land uplift to land submergence near 9 ka BP, although there is a strong difference in amplitude as pointed out above.

The behaviour of the land uplift histories shown in Figs 8(c) and (d) is closely related to the characteristics of the forebulge. In Fig. 9 the land uplift for laterally homogeneous and heterogeneous earth models as a function of distance from the load centre is plotted. In Fig. 9(a) we compare the continental and oceanic reference models L01 and L02 for two different times outside the load. Both models represent deep-flow models; therefore, a prominent forebulge can be observed, which migrates inwards with time. A decrease in lithospheric thickness results in a larger amplitude of the forebulge with its maximum closer to the load margin. On the introduction of a laterally homogeneous low-viscosity asthenosphere in the continental reference model L01 with $\eta_2 = 10^{19}$ Pa s, L01-19 in Fig. 9(b), the forebulge becomes less pronounced and migrates outwards with time, as expected for a channel-flow model (e.g. Wu 1993). On decreasing the asthenospheric viscosity further to $\eta_2 = 10^{18}$ Pa s (L01-18), the height of the forebulge decreases too. Next we discuss the forebulge behaviour for the laterally heterogeneous models LV2 and LV3, which both represent mixed-flow models with deep flow underneath the load and channel flow farther outside. In Fig. 9(c) we notice that the height of the forebulge for model LV2 has decreased by about two-thirds relative to model L01; the amplitudes are now closer to those for model L01-19. The bulge continues to migrate inwards, thus showing characteristics of both deep and channel flows. The inclusion of a lithospheric thickness

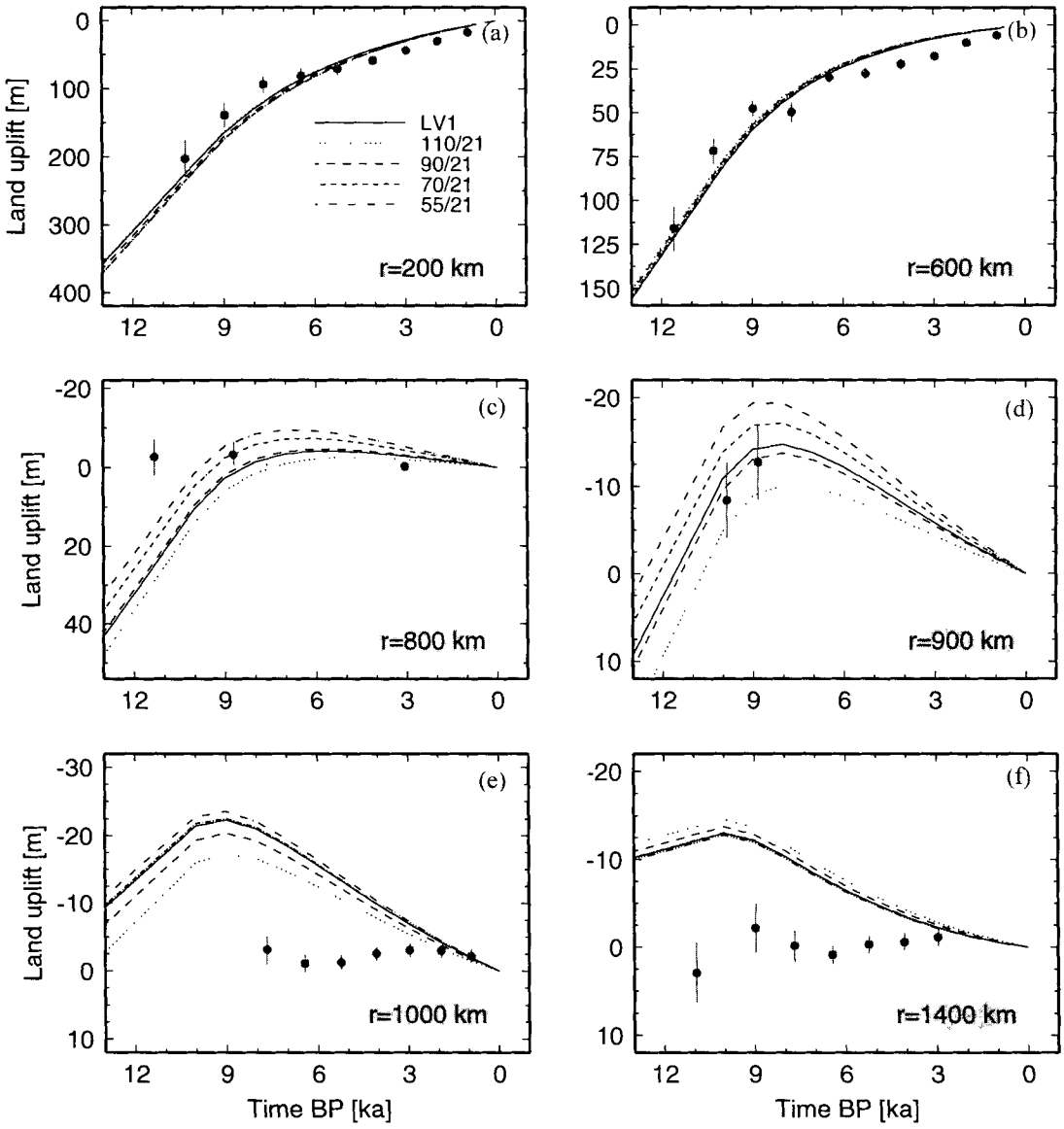

Figure 11. Land uplift as a function of time BP for the models LV1, 110/21, 90/21, 70/21 and 55/21 at the observation points $r = 200$ km (a), 600 km (b), 800 km (c), 900 km (d), 1000 km (e), and 1400 km (f). The line styles for the models are given in (a). Dots and bars represent observations and related uncertainties for Kristiinankaupunki (a), Helsinki (b), Kiel Bay (c), Korsør (d), Lübeck (e), and Leeuwarden (f).

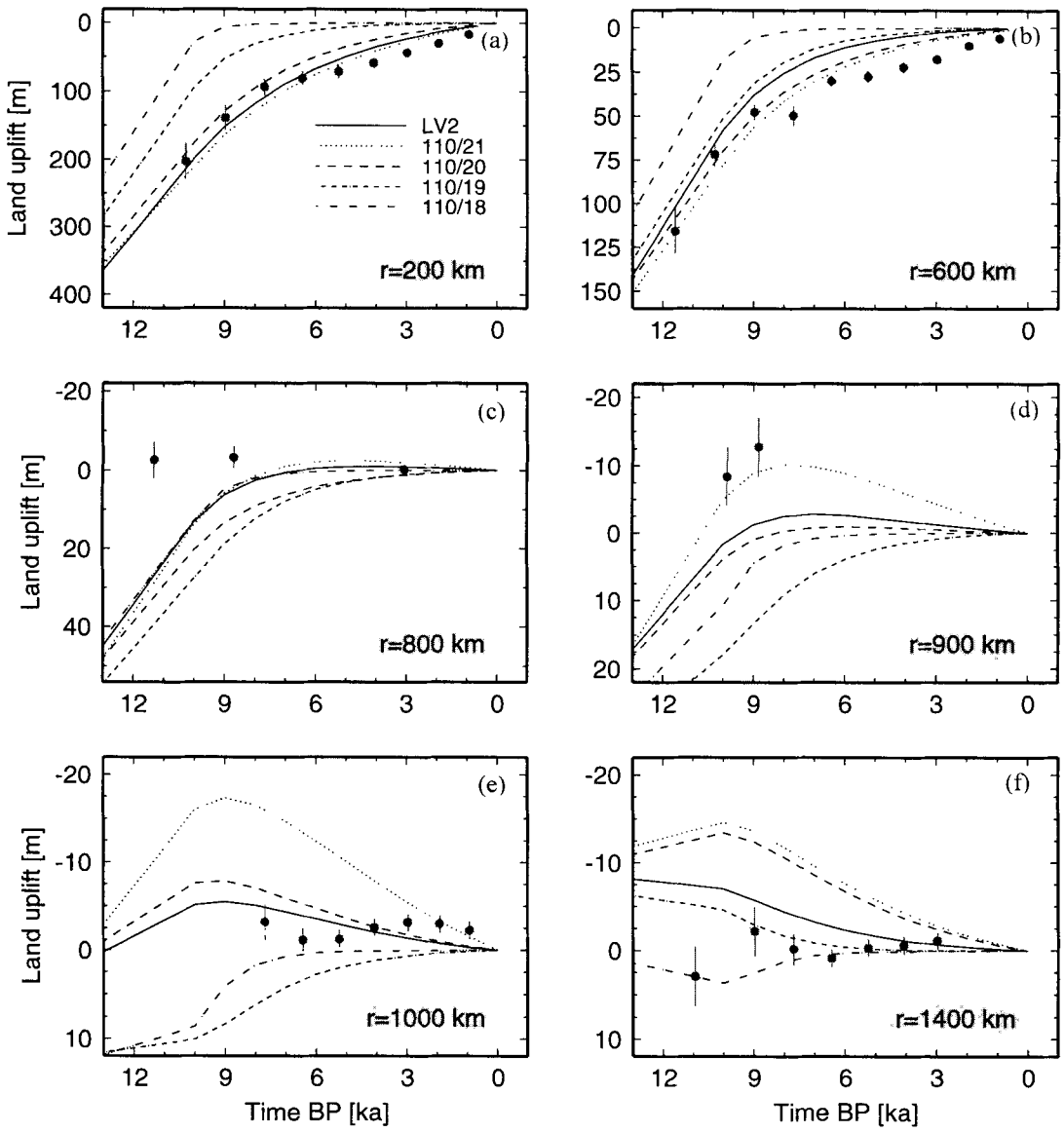

Figure 12. As Fig. 11, except that the calculations apply to models LV2, 110/21, 110/20, 110/19 and 110/18.

variation in model LV3 (Fig. 9d) increases the amplitude of the forebulge relative to model LV2 slightly, an effect resulting from the thinner lithosphere under the load margin and outside the load as discussed above.

Summarizing the effects of lateral heterogeneities for the linear loading cycle, we find that the assumption of lateral variations in the lithosphere and asthenosphere can significantly influence the predicted land uplift in formerly glaciated areas. Adopting a lateral variation in lithospheric thickness and asthenospheric viscosity as in models LV2 and LV3, which can be regarded as simple approximations of the rheology across a continental margin, the predicted land uplift around the load margin is modified (steeper curvature inside the load margin, decrease in forebulge), while the predicted land uplift in the central area of the formerly glaciated region remains unaffected. Thus, if we regard the Pleistocene ice sheet as known, we can resolve lateral heterogeneities in the upper mantle. On the other hand, a poorly known ice-sheet distribution can only be better constrained using relative sea-level predictions if both the radial and lateral structure of the rheology is known.

3.3 Comparison of homogeneous and heterogeneous earth models

In this section, we test the possibility of using sets of *laterally homogeneous*, layered earth models to infer lateral heterogeneities in the lithosphere and asthenosphere from postglacial land emergence data. Therefore the calculated land uplift for models LV1, LV2 and LV3 will be compared with calculations based on laterally homogeneous models. These models consist of an elastic lithosphere, a viscoelastic asthenosphere, and a viscoelastic mantle. Lithospheric thickness h_1 and asthenospheric viscosity η_2 are taken as free parameters, and the remaining parameter values are listed in Table 1. All models are drawn in Fig. 10; the laterally homogeneous models are

referred to as model x/y, with $h_1 = x$ km and $\eta_2 = 10^y$ Pa s. As in Section 3.2, we compare our predicted land uplift curves with selected observations from Scandinavia.

All results shown here are based on the finite-element method. In addition, the results for the laterally homogeneous models have been compared with corresponding calculations based on a spectral approach (e.g. Wolf 1985b). The differences between the calculated land uplift for both methods are only minor.

As a first step we investigate the case where there is only a lateral variation in lithospheric thickness. Therefore in Fig. 11 the calculated land uplift as a function of time is plotted for models LV1, 110/21, 90/21, 70/21, and 55/21 for six different distances from the load centre. For all models the asthenospheric viscosity has a value of 10^{21} Pa s. In the loaded area at the observation sites $r = 200$ and 600 km, the relative differences between the land uplifts for all models are only minor and it is not possible to resolve the lithospheric thickness. The observations can be explained by all earth models considered, a result that has also been established for predictions of land uplift near the centre of the Fennoscandian ice sheet (Wolf 1987). At the load margin ($r = 800$ km), the predicted land uplift for particular models is more distinct: here the land uplift for the heterogeneous model LV1 is closer to that for the homogeneous model 90/21. Moving farther out to $r = 900$ km, the land uplift curve for model LV1 lies between those for models 90/21 and 70/21, thus showing the influence of the thinner lithosphere at this location. At $r = 1000$ km, the response for model LV1 again shifts closer to that for model 70/21. At $r = 1400$ km, the uplift for model LV1 can be approximated by the uplift for model 70/21 or 55/21. Again the lithospheric thickness of these homogeneous models is similar to the value of model LV1 at this location, but the predicted land uplifts for the models are too similar to be distinguished within the observational uncertainties. To summarize, Figs 11(c)–(e) show that no laterally homogeneous model can

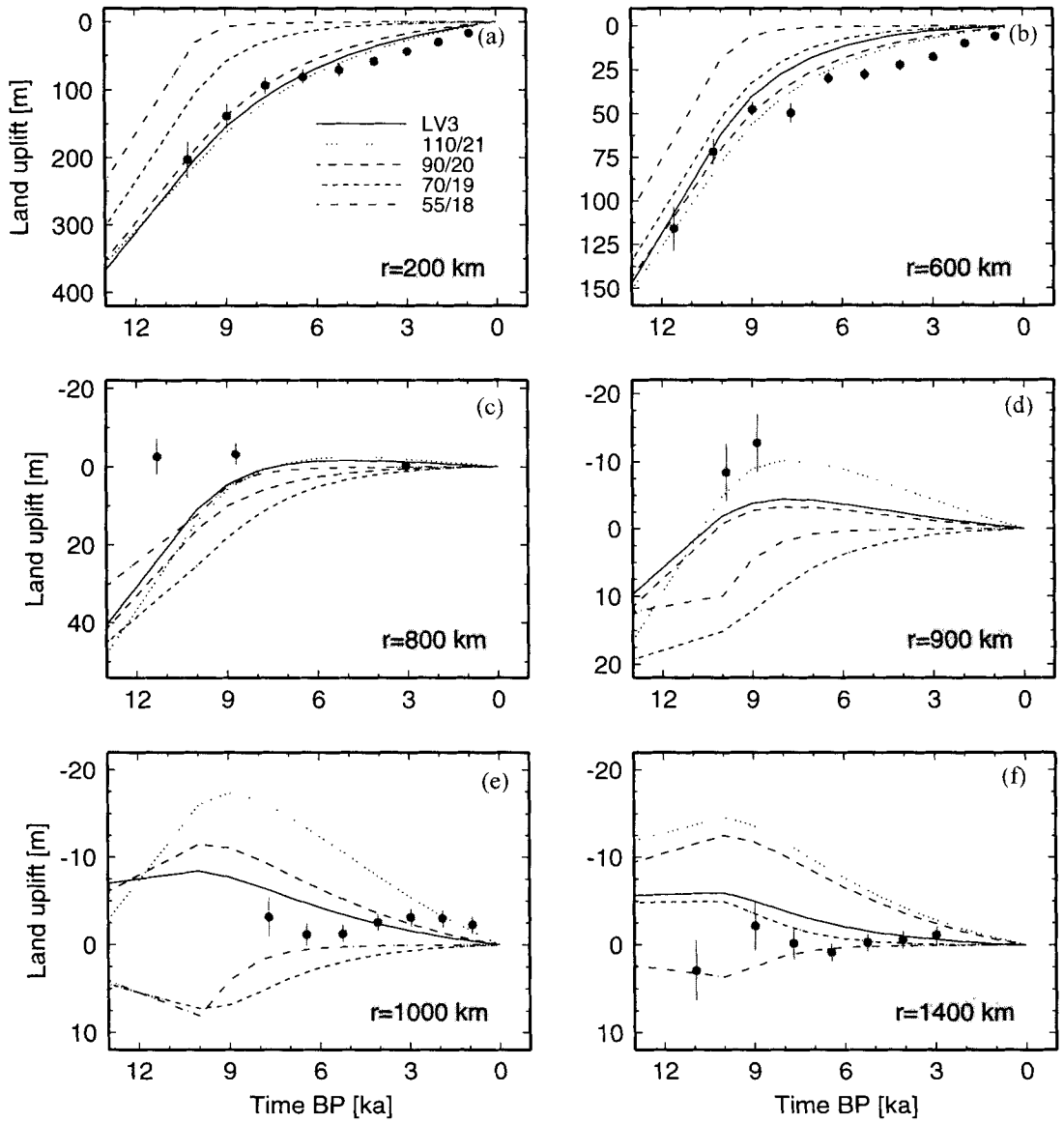

Figure 13. As Fig. 11, except that the calculations apply to models LV3, 110/21, 90/20, 70/19 and 55/18.

fit the land uplift predicted from model LV1 at all sites simultaneously. Moreover, the thickness of the lithosphere at any location can be inferred accurately by using laterally homogeneous models, when the lateral heterogeneity is restricted to variations in lithospheric thickness.

Next, we proceed to the case where there is only a lateral variation in asthenospheric viscosity. In Fig. 12 the calculated land uplift as a function of time is plotted for models LV2, 110/21, 110/20, 110/19 and 110/18 for six different distances from the load centre. Contrary to what has been found for the preceeding case (Fig. 11), the uplift in the loaded area can be used to determine the viscosity in the asthenosphere. An inspection of Fig. 12 indicates that the land uplift of model LV2 is close to that for model 110/21 near the load centre, and to that for model 110/19 at $r = 600$ km. At both locations the land uplift for model LV2 is smaller than that determined for the homogeneous model with values for h_1 and η_2 similar to those for model LV2 under the observation site, thus indicating that the weaker asthenosphere outside the loaded area contributes to the land uplift within. When we proceed towards the load margin and farther out (Figs 12c–f), the land uplift for model LV2 is significantly reduced due to the low-viscosity asthenosphere (Fig. 9). In particular, the land uplift for the heterogeneous model in the forebulge region can be better described using channel-flow models 110/20 and 110/19. Again, Fig. 12 indicates quite clearly that no laterally homogeneous model can fit the land uplift predicted by model LV2 at all sites simultaneously. However, the value of asthenospheric viscosity cannot be accurately inferred using laterally homogeneous models, especially for sites at or beyond the load margin, because the high-viscosity region underneath the load still influences the land uplift outside the loaded area.

Finally, we consider the case of lateral variations both in lithospheric thickness and asthenospheric viscosity. In Fig. 13, the calculated land uplift as a function of time is plotted for models LV3, 110/21, 90/20, 70/19 and 55/18 for six different distances from the load centre. At $r = 200$ km, the land uplift for model LV3 can be adequately approximated by the uplift for model 110/21. At $r = 600$ km, the uplift curve for model LV3 is between those for models 90/20 and 70/19, reflecting the fact that both the high-viscosity region underneath the load and the low-viscosity asthenosphere outside the loaded area contribute to the land uplift. This is consistent with the results of Fig. 11, which show that the effect of the lithosphere is negligible for both regions. The effect of the high-viscosity asthenosphere close to the load centre for model LV3 becomes more significant at $r = 900$ and 1000 km. Here, the land uplift for model LV3 is smaller than that for model 70/19, which is the laterally homogeneous model with values of h_1 and η_2 similar to those of model LV3 at this particular observation site. At $r = 1400$ km, the land uplift for model LV3 is close to the uplift for model 70/19. Comparing Figs 11–13, we conclude that the lateral variation in asthenospheric viscosity is the dominant feature, the thickness variation of the lithosphere has a negligible effect, and thus the remarks of Fig. 12 also apply, namely that lateral heterogeneity in the earth model exists but neither the viscosity of the asthenosphere nor the thickness of the lithosphere can be determined accurately using laterally homogeneous models.

The results can be summarized as follows. On the one hand, the inference of pure lateral variations in lithospheric thickness through the interpretation of land uplift observations with laterally homogeneous earth models is only possible *beyond* the load margin. On the other hand, a lateral variation in asthenospheric viscosity can be detected both within and outside the loaded area due to the larger percentage difference in land uplift for deep-flow and channel-flow models. However, we cannot quantify the lateral structure in the asthenosphere from the interpretation of relative sea-level observations alone. We note that these results only apply to the earth models tested in this study. A major restriction on the resolving power for the lateral heterogeneities considered in this paper arises from the uncertainties related to the observed land uplift. These uncertainties limit the detection of lateral heterogeneity, especially for models where only a lateral variation in lithospheric thickness is considered.

4 CONCLUSIONS

The results of the present study can be summarized as follows.

(1) Lateral heterogeneities in the lithosphere and asthenosphere can significantly influence the calculated land uplift in formerly glaciated areas for the load model considered.

(2) Lateral variations in lithospheric thickness, for example continental roots, influence land uplift predictions mainly in the area where the thickness is changing. These lateral variations can be resolved through observations of postglacial land emergence near the load margin and in the peripheral region.

(3) Lateral variations in the asthenosphere influence land uplift predictions both inside and outside the loaded area. However, lateral heterogeneities are most easily detected around the load margin and in the forebulge area.

(4) For earth models with lateral variations only in lithospheric thickness we can resolve the variation using laterally *homogeneous* models.

(5) For earth models with lateral variations in asthenospheric viscosity, the interpretation of postglacial land emergence based on laterally *homogeneous* models can only be used to establish the existence of lateral heterogeneities. The values of the asthenospheric viscosity and the lithospheric thickness cannot be resolved accurately. Thus, in order to infer these values correctly, we have to adopt laterally heterogeneous models for the interpretation.

We note that these results only apply to the range of earth and load models considered, and cannot be extended to other models without further study.

ACKNOWLEDGMENTS

We would like to thank W. Fjeldskaar and an anonymous reviewer for constructive comments on an earlier version of this manuscript. The figures in this paper were drawn using the GMT graphics package (see Wessel & Smith 1991 for details).

REFERENCES

Amelung, F. & Wolf, D., 1994. Viscoelastic perturbations of the Earth: significance of the incremental gravitational force in models of glacial isostasy, *Geophys. J. Int.*, **117**, 864–879.

Breuer, D. & Wolf, D., 1995. Deglacial land emergence and lateral upper-mantle heterogeneity in the Svalbard Archipelago—I. First results for simple load models, *Geophys. J. Int.*, **121**, 775–788.

Cathles, L. M., 1975. *The Viscosity of the Earth's Mantle*, Princeton University Press, Princeton, NJ.

Daly, R. A., 1934. *The Changing World of the Ice Age*, Yale University Press, New Haven, CN.

Fjeldskaar, W., 1994. Viscosity and thickness of the asthenosphere detected from the Fennoscandian uplift, *Earth planet. Sci. Lett.*, **126,** 399–410.

Gasperini, P. & Sabadini, R., 1989. Lateral heterogeneities in mantle viscosity and post-glacial rebound, *Geophys. J.*, **98,** 413–428.

Gasperini, P., Sabadini, R., & Yuen, D. A., 1991. Deep continental roots: the effects of lateral variations of viscosity on post-glacial rebound, in *Glacial Isostasy, Sea-Level and Mantle Rheology*, pp. 21–32, eds Sabadini, R., Lambeck, K., & Boschi, E., Kluwer, Dordrecht.

Haskell, N. A., 1935. The motion of a viscous fluid under a surface load, *Physics*, **6,** 265–269.

Jamieson, T. F., 1865. On the history of the last geological changes in Scotland, *Q. J. geol. Soc. Lond.*, **21,** 161–203.

Kaufmann, G. & Wolf, D., 1996. Deglacial land emergence and lateral upper-mantle heterogeneity in the Svalbard Archipelago—II. Extended results for high-resolution load models, *Geophys. J. Int.*, **127,** 125–140.

Lambeck, K., Johnston, P., & Nakada, M., 1990. Holocene glacial rebound and sea-level change in NW Europe, *Geophys. J. Int.*, **103,** 451–468.

Love, A. E. H., 1911. *Some Problems of Geodynamics*, Cambridge University Press, Cambridge.

McConnell, R. K., 1968. Viscosity of the mantle from relaxation time spectra of isostatic adjustment, *J. geophys. Res.*, **73,** 7089–7105.

Mitrovica, J. X. & Peltier, W. R., 1992. Constraints on mantle viscosity from relative sea level variations in Hudson Bay, *Geophys. Res. Lett.*, **19,** 1185–1188.

Mitrovica, J. X. & Peltier, W. R., 1993. The inference of mantle viscosity from an inversion of the Fennoscandian relaxation spectrum, *Geophys. J. Int.*, **114,** 45–62.

Nakada, M. & Lambeck, K., 1989. Late Pleistocene and Holocene sea-level change in the Australian region and mantle rheology, *Geophys. J.*, **96,** 497–517.

Nakada, M. & Lambeck, K., 1991. Late Pleistocene and Holocene sea-level change; evidence for lateral mantle viscosity structure?, in *Glacial Isostasy, Sea-Level and Mantle Rheology*, pp. 79–94, eds Sabadini. R, Lambeck. K & Boschi. E., Kluwer, Dordrecht.

Nataf, H. C. & Ricard, Y., 1996. 3SMAC: an a priori tomographic model of the upper mantle based on geophysical modeling, *Phys. Earth planet. Inter.*, **95,** 101–121.

Nataf, H. C. & Richter, F. M., 1982. Convection experiments in fluids with highly temperature-dependent viscosity and the thermal evolution of the planets, *Phys. Earth planet. Inter.*, **29,** 320–329.

Peltier, W. R., 1974. The impulse response of a Maxwell Earth, *Rev. geophys. Space Sci.*, **12,** 649–669.

Sabadini, R. & Gasperini, P. 1989. Glacial isostasy and the interplay between upper and lower mantle lateral viscosity heterogeneities, *Geophys. Res. Lett.*, **16,** 429–432.

Sabadini, R., Yuen, D. A. & Portney, M., 1986. The effects of upper mantle lateral heterogeneities on postglacial rebound, *Geophys. Res. Lett.*, **13,** 337–340.

Spiteri, R., 1991. Modelling the Alberta Foreland Basin, *MSc thesis*, University of Calgary, Calgary.

Tanimoto, T., 1990. Lateral variation of Q from singlet modal Q measurements of ${}_0S_2$, *Geophys. Res. Lett.*, **17,** 669–672.

Tushingham, A. M. & Peltier, W. R., 1991. Ice-3G: a new global model of late Pleistocene deglaciation based upon geophysical predictions of post-glacial relative sea level change, *J. geophys. Res.*, **96,** 4497–4523.

van Bemmelen, R. W. & Berlage, H. P., 1935. Versuch einer mathematischen Behandlung geotektonischer Bewegungen unter besonderer Berücksichtigung der Undationstheorie, *Gerlands Beitr. Geophys.*, **42,** 19–55.

Wessel, P. & Smith, W. H. F., 1991. Free software helps map and display data, *EOS, Trans. Am. geophys. Un.*, **72,** 441–446.

Wolf, D., 1984. The relaxation of spherical and flat Maxwell Earth models and effects due to the presence of the lithosphere, *J. Geophys.*, **56,** 24–33.

Wolf, D., 1985a. The normal modes of a uniform, compressible Maxwell half-space, *J. Geophys.*, **56,** 100–105.

Wolf, D., 1985b. The normal modes of a layered, incompressible Maxwell half-space, *J. Geophys.*, **57,** 106–117.

Wolf, D., 1987. An upper bound on lithosphere thickness from glacio-isostatic adjustment in Fennoscandia, *J. Geophys.*, **61,** 141–149.

Wolf, D., 1993. The changing role of the lithosphere in models of glacial isostasy: a historical review, *Global planet. Change*, **8,** 95–106.

Woodhouse, J. H. & Dziewonski, A. M., 1984. Mapping the upper mantle: three-dimensional modeling of Earth structure by inversion of seismic waveforms, *J. geophys. Res.*, **89,** 5953–5986.

Wu, P., 1992a. Deformation of an incompressible viscoelastic flat Earth with power-law creep: a finite element approach, *Geophys. J. Int.*, **108,** 35–51.

Wu, P., 1992b. Viscoelastic versus viscous deformation and the advection of pre-stress, *Geophys. J. Int.*, **108,** 136–142.

Wu, P., 1993. Postglacial rebound in a power-law medium with axial symmetry and the existence of the transition zone in relative sea-level data, *Geophys. J. Int.*, **114,** 417–432.

Wu, P. & Peltier, W. R., 1982. Viscous gravitational relaxation, *Geophys. J. R. astr. Soc.*, **70,** 435–485.